

Supplementary Information for

**Electrical Readout of Light-Induced Spin Transition in Thin Film Spin Crossover/Graphene Heterostructure**

*Nikita Konstantinov<sup>1</sup>, Arthur Tauzin<sup>3</sup>, Ulrich Nguetchuissi Noubé<sup>1</sup>, Diana Dragoé<sup>3</sup>, Bohdan Kundys<sup>1</sup>, Hicham Majjad<sup>1</sup>, Arnaud Brosseau<sup>4</sup>, Marc Lenertz<sup>1</sup>, Aditya Singh<sup>1,5</sup>, Stéphane Berciaud<sup>1</sup>, Marie-Laure Boillot<sup>3</sup>, Bernard Doudin<sup>1\*</sup>, Talal Mallah<sup>3\*</sup> and Jean-Francois Dayen<sup>1,2\*</sup>.*

1. Université de Strasbourg, CNRS, Institut de Physique et Chimie des Matériaux de Strasbourg (IPCMS), UMR 7504, 23 rue du Loess, Strasbourg, 67034, France.
2. Institut Universitaire de France (IUF), 1 rue Descartes, 75231 Paris cedex 05, France.
3. Institut de Chimie Moléculaire et des Matériaux d'Orsay, Univ. Paris-Sud, Université Paris-Saclay, CNRS, UMR 8182, 91405 Orsay cedex, France.
4. ENS Paris-Saclay, Université Paris-Saclay, 4 av. des Sciences, CS 30008, 91192 Gif sur Yvette, France.
5. Department of Physics, Indian Institute of Technology Delhi, 110016, New Delhi, India.

To whom correspondence should be sent: [bernard.doudin@ipcms.unistra.fr](mailto:bernard.doudin@ipcms.unistra.fr) , [talal.mallah@universite-paris-saclay.fr](mailto:talal.mallah@universite-paris-saclay.fr) , [dayen@unistra.fr](mailto:dayen@unistra.fr)

## Table of content

1. Raman spectroscopy .....	2
2. Atomic Force Microscopy (AFM) imaging and profilometry .....	3
3. X-ray powder diffraction .....	4
4. X-ray Photoelectron Spectroscopy (XPS) .....	5
5. Reproducibility of thermal hysteresis conductance characteristics .....	6
6. Conductance versus temperature characterization of graphene substrate without spin crossover material .....	7
7. Photoconduction characterization of graphene/SCO heterostructure and graphene only devices	8
8. Successive conductance vs temperature cycles .....	9

## 1. Raman spectroscopy

**Figure S.1.a** shows (below) typical Raman spectra of SCO/Graphene (red) and bare Graphene (grey) showing the G- and 2D-mode features along with evidence for a fairly small intensity of the defect-induced D-mode. The spectra are vertically offset for clarity. **Figure S.2.b** shows correlation plot of the G- and 2D-mode frequencies ( $\omega_G$ ,  $\omega_{2D}$ ) extracted from a Raman map take on  $21 \times 21 \mu\text{m}^2$  areas on SCO/graphene (red disks) and bare graphene (grey disks). The red and black solid red lines both have a slope of  $\frac{\partial \omega_{2D}}{\partial \omega_G} = 1.4 \pm 0.1$  and are linear fit to the correlation plots in the SCO/graphene and bare graphene regions, respectively. The spatially averaged values (larger square symbols) and standard deviations (error bars) are indicated for both regions with the same color code. The two vectors in the inset indicate the slopes corresponding strain ( $\mathbf{e}_S$ , slope 2.2) and hole doping ( $\mathbf{e}_H$ , slope 0.7), allowing to separate strain- and doping-induced shifts as in reference [1]. The segment that connects the spatially averaged values on SCO/graphene and bare graphene has a slope near 1.1. Considering that bare graphene on  $\text{SiO}_2$  is typically hole doped, these measurements suggest that deposition of SCO molecules on graphene leads to slightly larger hole doping (by less than  $2 \times 10^{12} \text{ cm}^{-2}$ ) along with a minute compressive strain (of  $\sim 10^{-4}$ ), as compared to the bare graphene reference (ref.[2]).

Measurements were taken at 300 K under vacuum in on a home built  $\mu$ -Raman setup under laser illumination at 532 nm with a power below 1 mW to minimize sample heating.

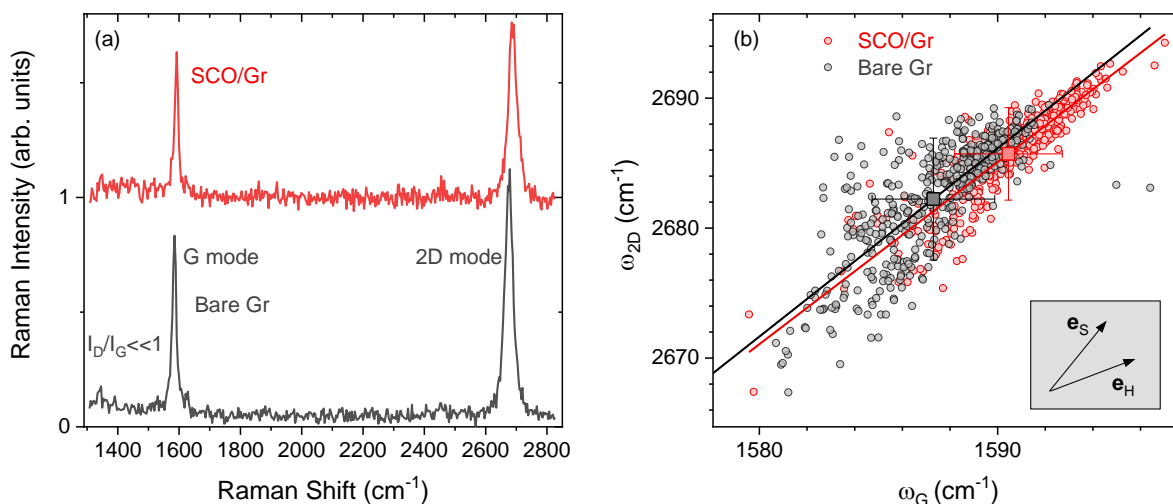


Figure S1. a) Typical Raman spectra of SCO/Graphene (red) and bare Graphene (grey) showing the G- and 2D-mode features along with evidence for a fairly small intensity of the defect-induced D-mode. The spectra are vertically offset for clarity. b) Correlation plot of the G- and 2D-mode frequencies ( $\omega_G$ ,  $\omega_{2D}$ ) extracted from a Raman map take on  $21 \times 21 \mu\text{m}^2$  areas on SCO/graphene (red disks) and bare graphene (grey disks). The spatially averaged values (larger square symbols) and standard deviations (error bars) are indicated for both regions with the same color code.

## 2. Atomic Force Microscopy (AFM) imaging and profilometry

AFM imaging of a  $2 \times 2 \mu\text{m}^2$  area window reveals the detailed structure of the film made of nanocrystals of different dimensions among them many have a platelet shape with thickness around 25 nm and surface that can be up to  $300 \times 400 \text{ nm}^2$  (**Figure S2a**). Profilometry allows measuring the thickness of the film over a large area, it confirms the AFM data (**Figure S2b**).

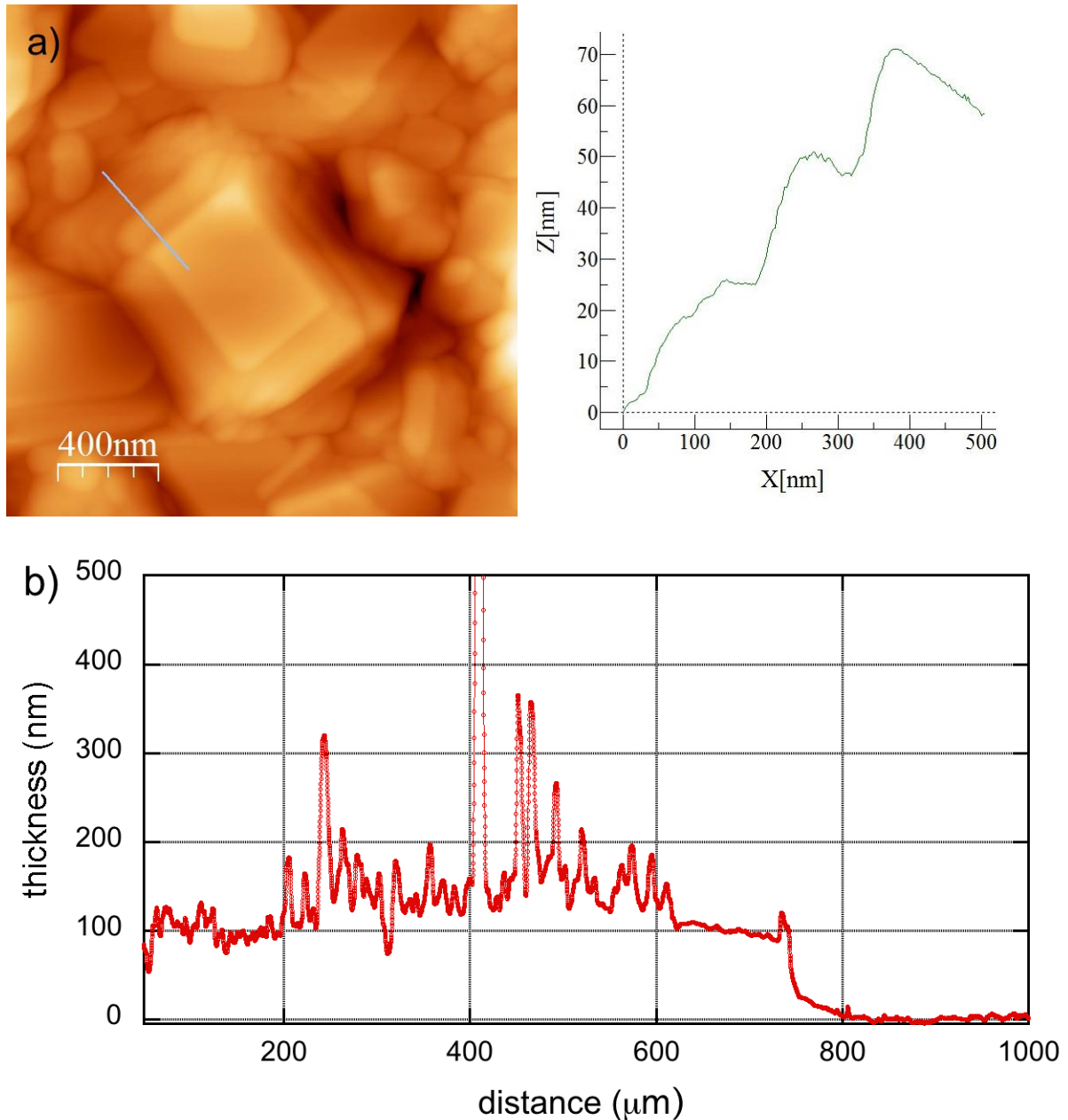


Figure S2. a) Topographic AFM image ( $2 \times 2 \mu\text{m}^2$ ) region showing steps of 25 nm and a nanocrystal surface around  $300 \times 400 \text{ nm}^2$ , b) Profilometry pattern of the SCO film deposited over graphene showing an average thickness around 120 nm.

### 3. X-ray powder diffraction

The X-ray diffraction was recorded in the  $\theta$ - $2\theta$  mode using a Rigaku Smartlab (9 kW) diffractometer in parallel beam geometry equipped with a Cu  $K_{\alpha 1}$  source ( $\lambda = 1.54059 \text{ \AA}$ ) and a Ge(220) 2-bounce front monochromator.

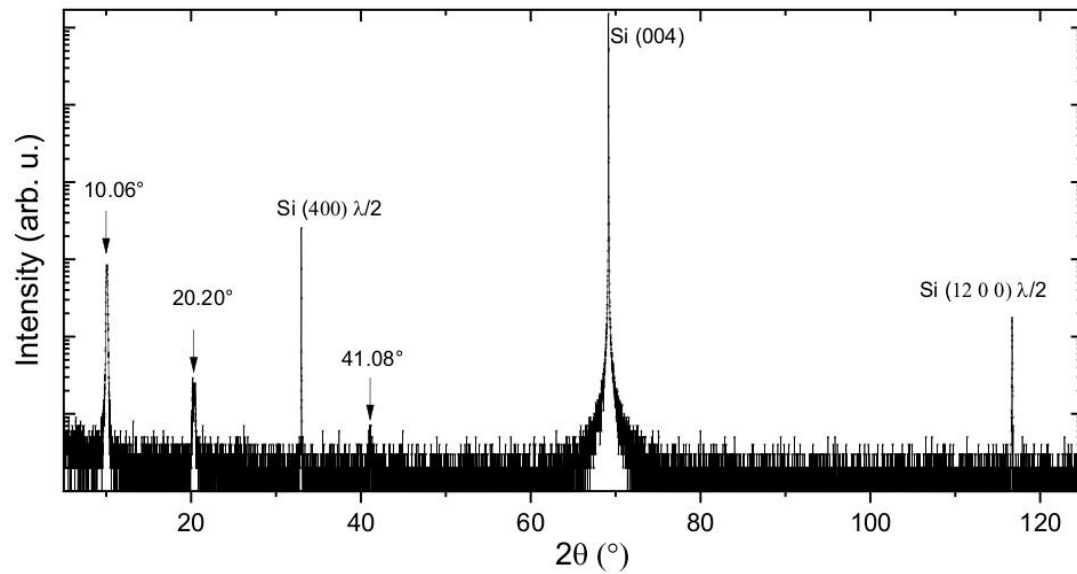


Figure S3. X-ray powder diffraction pattern of the film

## 4. X-ray Photoelectron Spectroscopy (XPS)

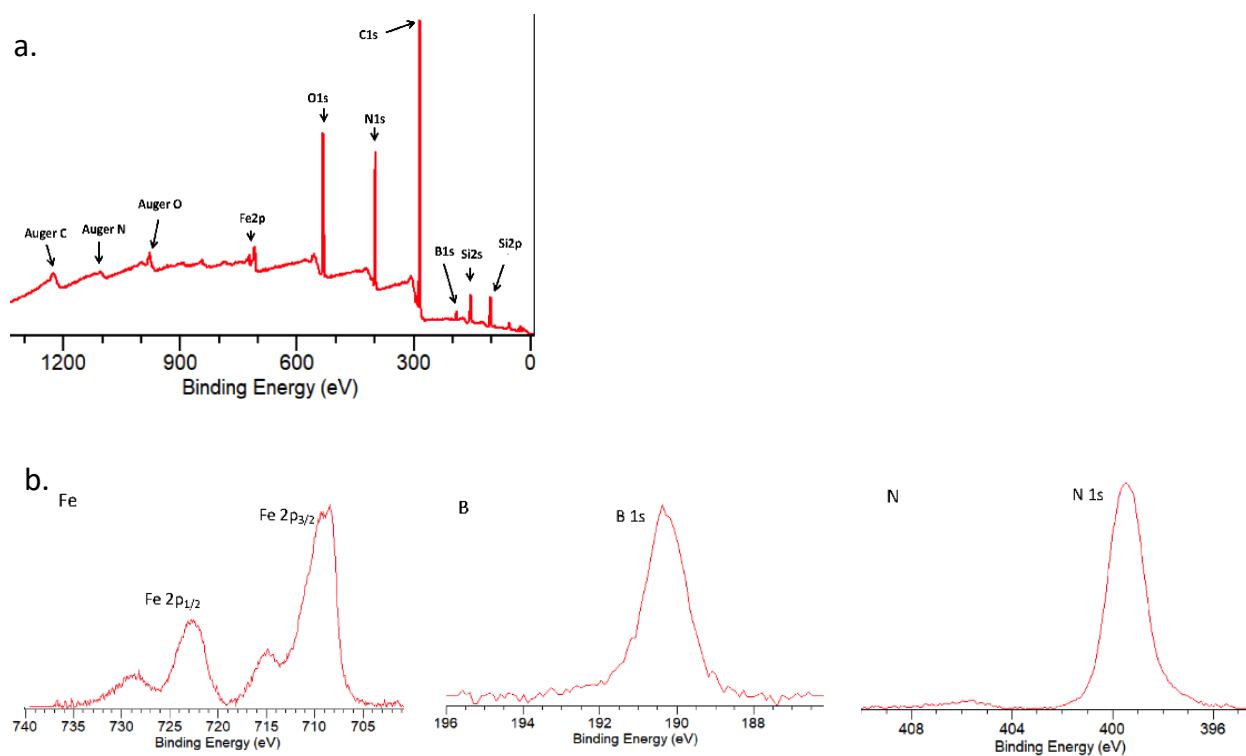


Figure S4. a) Survey XPS spectrum of the thin film showing the presence of all the elements of  $\text{Fe}[\text{HB}(3,5\text{-(Me)}_2\text{Pz)}_3]_2$ , b) XPS spectra of the thin film at the Fe (2p), B (1s) and N (1s) edges.

## 5. Reproducibility of thermal hysteresis conductance characteristics

We performed several conductance vs. temperature measurements on different devices made from the same SCO/Graphene sample. **Figure S5** reports derivatives of the conductance vs. temperature measurements ( $dG/dT(T)$ ), showing that the transition temperatures are reproducible with average values of  $T_{\downarrow} = 136 \pm 3$  K and  $T_{\uparrow} = 153 \pm 3$  K.

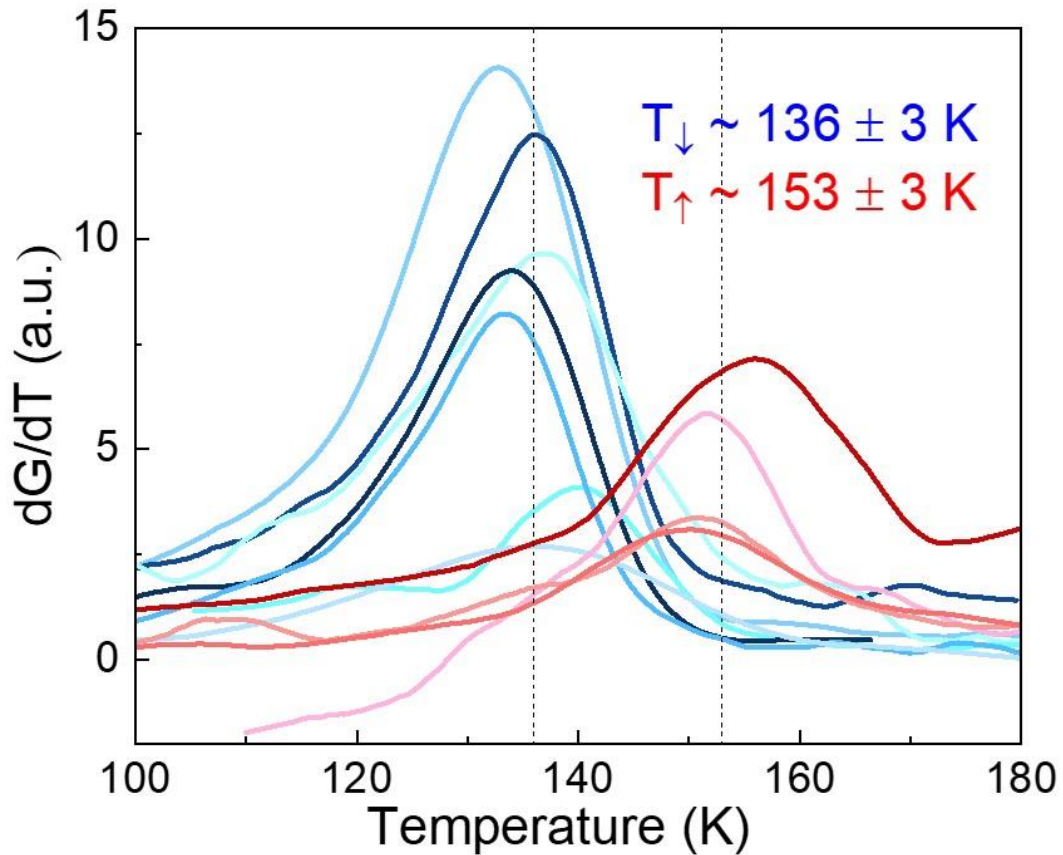
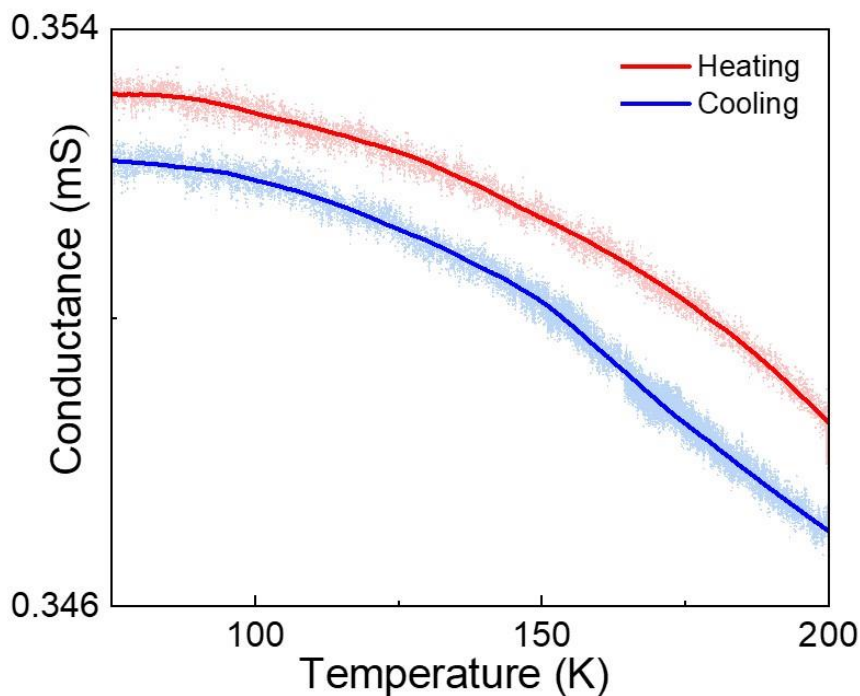


Figure S5.  $dG/dT$  vs. temperature plots for different devices of the same SCO/graphene sample.

## 6. Conductance versus temperature characterization of graphene substrate without spin crossover material

Graphene device was patterned in multi-terminals Hall bar geometry, from the same CVD graphene/SiO<sub>2</sub> substrate than the one used to fabricate the graphene/SCO heterostructures. The temperature dependence of the conductance resistance (at zero gate bias) of the bare graphene device is shown in **Figure S6**. The negative temperature dependence of the conductance in both heating (red curve) and cooling (blue curve) modes indicates a metallic behavior. The two curves retrace on each other with a 0.3% shift, confirming as, expected, the absence both of hysteresis and of thermal transition in the bare graphene substrate.



*Figure S6. Conductance (temperature) characteristics of a bare graphene reference device without SCO layer (under 3 mV DC excitation, at zero gate voltage). No hysteresis neither thermal transition is observed.*

## 7. Photoconduction characterization of graphene/SCO heterostructure and graphene only devices

**Figure S7** reports the photoconduction response to red light excitation (647 nm,  $550 \mu\text{W}\cdot\text{mm}^{-2}$ ) of a graphene only device (black dots) and a SCO/graphene heterostructures (brown dots). Both devices have been patterned with Hall bar geometry with identical geometrical parameters. Series of irradiation/relaxation steps of 15 minutes each at 10 K were performed for 4 hours. Reversible small changes of the resistance observed when switching the light on (green areas) and off (white areas) are observed on both samples, and are attributed to photo-thermoelectric effects at the Ti/Au contacts. The larger amplitude of the thermoelectric effect for the SCO/graphene heterostructures compared to the bare graphene traduces the difference in heat dissipation between the two systems. The relative change of conductance of the bare graphene device does not exceed  $-0.3\%$  after the 4 hours of experiments. On the contrary, the relative change of conductance of the SCO/graphene heterostructures is one decade higher, reaching mostly  $+4\%$  of remnant increase of the conductance, and is attributed to electrical transduction by the graphene channel of the LIESST effect taking place into the SCO layer (see dashed red line as guide for the eye).

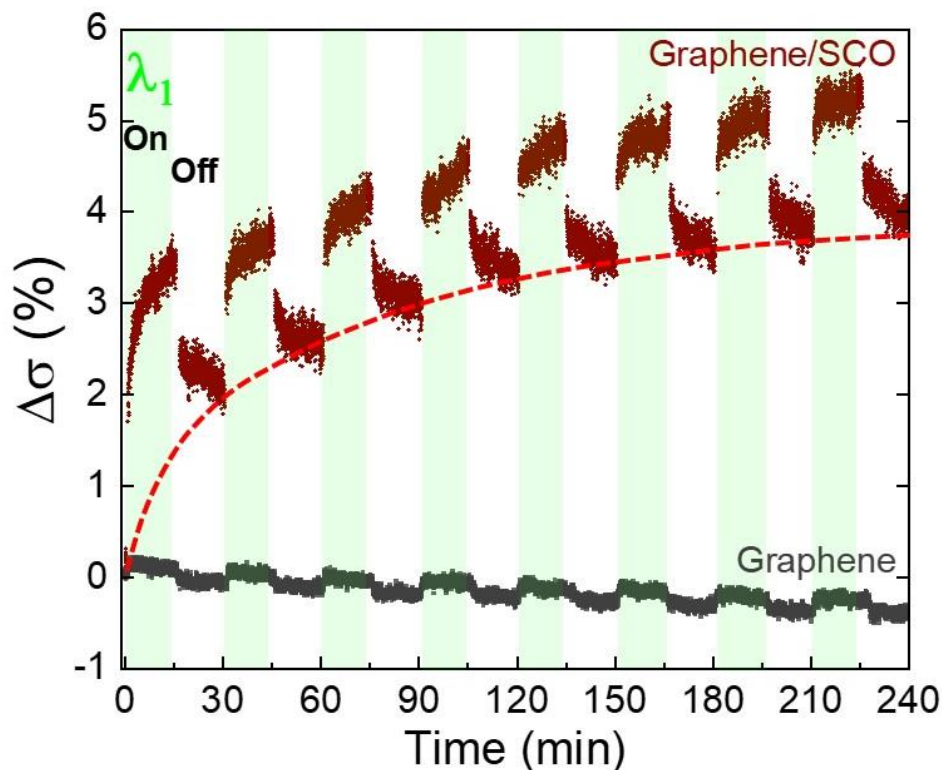


*Figure S7. Relative change of the conductance of graphene only device (black dots) and SCO/graphene heterostructures (brown dots) under series of red light (647 nm,  $550 \mu\text{W}\cdot\text{mm}^{-2}$ ) irradiation/relaxation steps of 15 minutes each at 10 K. Remnant change of the heterostructures conductance due to LIESST effect is observed (dashed red line), while bare graphene device conductance remains comparatively mostly unchanged.*

## 8. Successive conductance vs temperature cycles

We performed successive conductance vs. temperature cycles, showing the reproducibility and stability of the device upon thermal cycling, with preserved thermal spin transition, similar conductance levels reached in the HS and LS states, and reproducible shape of the thermal hysteresis.

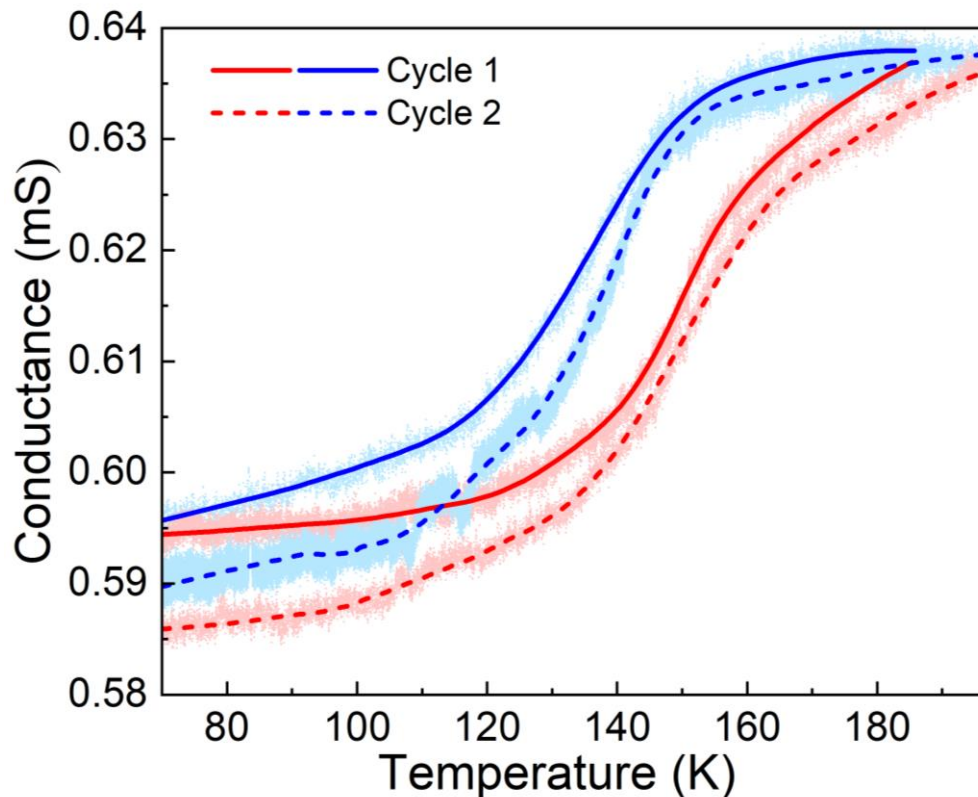


Figure S8. Conductance vs temperature cycles measured successively on a graphene/SCO devices.

References :

[1] Ji Eun Lee, Gwanghyun Ahn, Jihye Shim, Young Sik Lee & Sunmin Ry, Nature Communications, **2012**, 3, 1024.

[2] Guillaume Froehlicher and Stéphane Berciaud, Physical Review B., **2015**, 91, 205413.